Inorganic Chemistry

Article

pubs.acs.org/IC

# XRD Monitoring of $\alpha$ Self-Irradiation in Uranium−Americium Mixed Oxides

Denis Horlait,[†] Florent Lebreton,[†] Pascal Roussel,[‡] and Thibaud Delahaye*,[†]

[†]CEA, DEN, DTEC/SDTC/LEMA, F-30207 Bagnols-sur-Cèze Cedex, France

[‡]Unité de Catalyse et Chimie du Solide, UMR 8012 CNRS, Ecole Nationale Supérieure de Chimie de Lille BP 90108, 59652 Villeneuve d'Ascq Cedex, France

**ABSTRACT:** The structural evolution under $^{241}$Am self-irradiation of $U_{1-x}Am_xO_{2\pm\delta}$ transmutation fuels (with $x \leq 0.5$) was studied by X-ray diffraction (XRD). Samples first underwent a preliminary heat treatment performed under a reducing atmosphere (Ar/$H_2$(4%)) aiming to recover the previously accumulated structural defects. Over all measurements (carried out over up to a full year and for integrated doses up to $1.5 \times 10^{18}$ $\alpha$-decay events·g$^{-1}$), only fluorite $U_{1-x}Am_xO_{2\pm\delta}$ solid solutions were observed. Within a few days after the end of the heat treatment, each of the five studied samples was slowly oxidized as a consequence of their move to air atmosphere, which is evidenced by XRD by an initial sharp decrease of the unit cell parameter. For the compounds with $x \leq 0.15$, this oxidation occurred without any phase transitions, but for $U_{0.6}Am_{0.4}O_{2\pm\delta}$ and $U_{0.5}Am_{0.5}O_{2\pm\delta}$, this process is accompanied by a transition from a first fluorite solid solution to a second oxidized one, as the latter is thermodynamically stable in ambient conditions. In the meantime and after the oxidation process, $^{241}$Am $\alpha$ self-irradiation caused a structural swelling up to ∼0.8 vol %, independently of the sample composition. The kinetic constants of swelling were also determined by regression of experimental data and are, as expected, dependent on $x$ and thus on the dose rate. The normalization of these kinetic constants by sample $\alpha$-activity, however, leads to very close swelling rates among the samples. Finally, evolutions of microstrain and crystallite size were also monitored, but for the considered dose rates and cumulated doses, $\alpha$ self-irradiation was found, within the limits of the diffractometer used, to have almost no impact on these characteristics. Microstrain was found to be influenced instead by the americium content in the materials (i.e., by the impurities associated with americium starting material and the increase of cationic charge heterogeneity with increasing americium content).

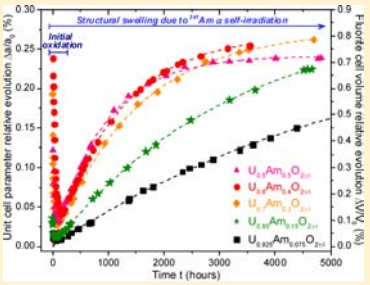


## 1. INTRODUCTION

Minor actinides (neptunium, americium, and curium) are generated in UOX (uranium oxide) and MOX (mixed U−Pu oxides) fuels during their irradiation in reactors. Though these elements represent a very low fraction in spent nuclear fuels (<0.1 wt %), their high activity and long half-life make them the major contributors to radioactivity in nuclear waste beyond 100 years (if the choice is made to recycle plutonium in MOX fuels). In order to reduce the radiotoxicity of nuclear waste, the transmutation of minor actinides (MA) into short-lived elements is currently evaluated in the framework of fast neutron reactor (FNR) development.[1] At the current time, uranium-based $U_{1-x}MA_xO_{2\pm\delta}$ mixed oxides appear, for France, to be the most promising fuels for performing the transmutation of minor actinides. In detail, two specific modes are considered and studied.[2−7] The first one is the homogeneous mode and consists of irradiating fuels containing a low amount of MA (<5% of the heavy metals), which constitute the overall core. On the other hand, the heterogeneous mode, which has nowadays become the reference mode, consists of integrating MA in specific oxides destined to be placed in the core periphery, therefore called minor actinide-bearing blanket (MABB). To that end, MA are integrated in $U_{1-x}MA_xO_{2\pm\delta}$ mixed oxides in relatively high concentrations (7 to 20 at. % of the heavy metals). Since Am is dominant in terms of activity and heat load compared to the other MA, the current research is mainly focused on $U_{1-x}Am_xO_{2\pm\delta}$ compounds.

Before an effective industrial deployment, numerous points need, however, to be clarified concerning $U_{1-x}Am_xO_{2\pm\delta}$ properties. For example, even though the stake of MA transmutation has been motivating substantial studies on the $U_{1-x}Am_xO_{2\pm\delta}$ solid solutions,[4−20] even including irradiation experiments,[6,21] little experimental data about self-irradiation effects in $U_{1-x}Am_xO_{2\pm\delta}$ exists.[22−24] Self-irradiation effects are of great concern because the probable local modifications induced (lattice swelling, amorphization, phase transition, He formation, etc.) could cause modifications at the macroscopic scale such as pellet swelling, brittleness, and grains fracturation, which would eventually have consequences on the fuel handling (e.g., cladding) and its properties (thermal conductivity, in-pile microstructure evolution, etc.).

Thus, to assess the behavior under $\alpha$ self-irradiation of uranium−americium mixed oxides, five $U_{1-x}Am_xO_{2\pm\delta}$ compounds (with $x$ = 0.075, 0.15, 0.3, 0.4, and 0.5) were monitored by XRD to study the effect at the crystal lattice scale. This

**Received:** August 20, 2013
**Published:** November 22, 2013

  

monitoring was performed over a full year, with cumulated doses up to $1.5 \times 10^{18}$ $\alpha$-decay events·g$^{-1}$, that is, about 0.37 dpa (displacements per atom).

## 2. EXPERIMENTAL SECTION

**2.1. Sample Preparation.** All sample preparation was performed in hot cells and glove boxes at the CEA Marcoule ATALANTE facility. The five samples of $U_{1-x}Am_xO_{2\pm\delta}$ were prepared from $UO_{2+\delta}$ and $^{241}AmO_{2-\delta}$ starting powders, following the recently developed UMACS (uranium minor actinide conventional sintering) process.[6,25] This process consists of two successive heat treatments (the first aiming to form the solid solution, the second for sintering) on pelletized powders, separated by a grinding step. As information on starting powder characteristics[6,8] and the fabrication process[6] were already given in previous studies, they are not further described herein.

The Am/(U+Am) ratio (Table 1) and impurity content of each sintered sample were determined using TIMS (thermal ionization mass spectrometry). As expected, Np constitutes the main impurity (Np/(Am+Np) is about 0.4%) as $^{237}$Np is the long-lived decay product of $^{241}$Am. Other impurities were detected, but at their level (1000 ppm for all impurities cumulated[6]), we assume that they should not interfere with sample evolution under self-irradiation. More detailed characterization of the samples with $x = 0.075$ on one hand, and with $0.15 \leq x \leq 0.5$ on the other, is available in two recent publications, refs 6 and 26, respectively.

**Table 1. Sample Compositions (Determined by TIMS) and Total Experiment Durations Expressed in Time, Cumulated $\alpha$ Dose, and dpa (Displacements Per Atom)**

| $x$ (Am/(U+Am)) | | | cumulated dose | |
|---|---|---|---|---|
| targeted | obtained | experiment duration (days) | $\alpha$·g$^{-1}$ | dpa[a] |
| 0.075 | 0.075(5) | 484 | $3.5 \times 10^{17}$ | 0.08 |
| 0.15 | 0.15(1) | 307 | $4.4 \times 10^{17}$ | 0.11 |
| 0.30 | 0.32(1) | 317 | $1.0 \times 10^{18}$ | 0.24 |
| 0.40 | 0.39(1) | 268 | $1.0 \times 10^{18}$ | 0.24 |
| 0.50 | 0.49(1) | 322 | $1.5 \times 10^{18}$ | 0.37 |

[a]dpa were calculated considering 1600 displacements for each $^{241}$Am $\alpha$ decay.[31,42]

After fabrication, a fragment (a few tens of milligrams) of each obtained pellet was heat treated in a furnace to anneal the self-irradiation effects accumulated since fabrication, before starting the XRD experiments. This treatment under an Ar/$H_2$(4%) flow was composed of a half-hour plateau at 1373 K reached with a heating rate of 10 K·min$^{-1}$ and followed by a cooling at 25 K·min$^{-1}$ to room temperature. In order to fully recover the self-irradiation defects, the plateau temperature was selected considering the recovery temperature usually reported for actinide oxides.[27−30] The chosen value was also a posteriori ensured by the recent work of Prieur et al. on thermal recovery of defects of $U_{0.8}Am_{0.2}O_{2-\delta}$, as they obtained a defect-free sample after holding a few minutes at this temperature.[23] The moment when the sample is cooled to room temperature is hence considered to be the experiment start time, called $t_0$. The sample is then manually ground in an agate mortar, embedded in organic grease, and finally layer-deposited on a silicon mirror plate sample holder.

**2.2. XRD.** *2.2.1. Measurements.* XRD patterns were recorded using a Bruker D8 Advance diffractometer equipped with a special sealed sample holder for radioactive compound measurements notably equipped with a beryllium window transparent to X-rays though ensuring sample containment. The source is Cu ($K\alpha_{1,2}$ radiation, $\lambda_1$ = 1.5406 Å) and the detector a linear Lynx-Eye.

The diffractograms were collected from 25 to 120° ($\theta$−$2\theta$ mode). A step of 0.0105° ($2\theta$) and a counting time of 1.15 s·step$^{-1}$ were considered and led to a 3 h recording time. During the first ∼100 h of each experiment, as the 3 h recording time could not be neglected compared to the aging of the sample, shorter counting times (0.19, 0.38, or 0.57 s·step$^{-1}$) were preferred to reduce the diffractogram recording times to, respectively, 0.5, 1, or 1.5 h.

Any potential instrumental deviation was continuously controlled by adding a gold powder (Sigma-Aldrich, > 99.9%) as an internal standard on each sample plate (gold was initially mixed with the grease). This standard was also used as a reference for $2\theta$ positioning and normalization of diffraction line relative intensities.

*2.2.2. Data Processing. 2.2.2.1. Unit Cell Parameter Determination.* To determine the unit cell parameters, the Fullprof Suite[32] software was employed, and a modified Thompson−Cox−Hastings Pseudo-Voigt profile function (TCH-Z) was selected in order to take into account the possible microstructural changes of the samples (strain and size effects). As this kind of refinement requires the subtraction of the XRD device contribution to line broadening, a dedicated $LaB_6$ SRM660b microcrystalline standard powder (provided by the National Institute of Standards and Technology (NIST)) was regularly analyzed. No abnormal deviations of the obtained pattern characteristics were observed, which confirmed the stability of the XRD apparatus during the experiment.

*2.2.2.2. Microstrain and Average Crystallite Size Determination.* Powder XRD line broadening is the sum of several contributions. A first group of contributions only concerns the apparatus characteristics and has to be subtracted using a microcrystalline standard as described in the previous paragraph. The second group consists of contributions of the sample and contains two components: one contribution due to the finite size of the coherent domain (and hence directly related to the crystallite size) and another to the contribution of local microdistortions (i.e., microstrain), in other words, the local variations of interatomic distances (and thus of unit cell parameter).[33,34] To dissociate the line broadening due to crystallite size and microstrain, the well-established Williamson−Hall plot was employed.[33−36] This method is based on the fact that microstrains provoke a Gaussian-type diffraction line broadening, while decreased crystallite size brings about Lorentzian-type broadening. The two contributions could then be deconvoluted by writing, for one individual XRD peak:

$$\beta_{mat} = \beta_G + \beta_L = \lambda/(L\cos\theta) + 4(\tan\theta)\varepsilon \quad (1)$$

with $\beta_{mat}$, the integral breadth of the considered diffraction peak for the studied material, $\beta_G$ and $\beta_L$, respectively the Gaussian and Lorentzian contributions to integral breadth, $L$, the crystallite size, $\theta$, the angular position of a considered X-ray reflection (expressed in radians), and $\varepsilon$, the microstrain. The plotting of $\beta_{mat}\cos\theta$ values for each individual and well-defined diffraction line as a function of $\sin\theta$ then directly gives access to the mean value of microstrain $\langle\varepsilon\rangle$ and to the crystallite size $L$, as the slope and the intercept of the straight line, respectively, correspond to $\langle\varepsilon\rangle$ and to $\lambda$/L.

## 3. RESULTS AND DISCUSSION

**3.1. XRD Pattern Evolution.** During the first days of XRD monitoring, a quite singular evolution was noted for $U_{0.5}Am_{0.5}O_{2\pm\delta}$ and $U_{0.6}Am_{0.4}O_{2\pm\delta}$ compared to that observed for $U_{0.85}Am_{0.15}O_{2\pm\delta}$ and $U_{0.925}Am_{0.075}O_{2\pm\delta}$, while $U_{0.7}Am_{0.3}O_{2\pm\delta}$ exhibited a behavior considered intermediate. They are thus presented separately in sections 3.1.2, 3.1.3, and 3.1.4, respectively.

*3.1.1. Gold Reference.* Concerning the gold powder reference, similar behaviors were observed for each of the five samples. First, as expected, no broadening was noted, regardless of the sample or its aging, as evidenced, for example, in Figure 1 through the evolution of the Au (311) reflection. The angular position of gold diffraction lines were found to vary by less than 0.02°2$\theta$. As these shifts are completely random, they are only due to variations in the sample holder position. It also indicates that this reference phase does not quantifiably undergo the effects of $\alpha$-irradiation due to the proximity of the americium-bearing sample.


dx.doi.org/10.1021/ic402124s | Inorg. Chem. 2013, 52, 14196−14204

During the experiments, the intensities of the Au diffraction lines randomly vary by at maximum ±10% for all the samples, with the exception of $U_{0.5}Am_{0.5}O_{2\pm\delta}$, for which higher variations (±30%) were noted. As these variations of intensities are random, they could only be explained by an uneven spreading of the grease/Au/sample mixture on the sample holder and of an heterogeneity of the mixture itself.

In addition to the stochastic variation of diffraction line intensities, a slight progressive decrease (~15% over a full year) of the Au diffraction line intensities is also perceived. The latter is attributed to the decrease of the X-ray source intensity over time and is thus independent of sample evolution.

In summary, an Au reference could be used to normalize the diffraction line intensities and positions for all the samples (except for intensities of $U_{0.5}Am_{0.5}O_{2\pm\delta}$), as shown in Figures 1, 2, and 3. After this normalization, variations of the pattern characteristics (diffraction line positions, intensities, and peak profiles) are thus considered to be only related to the $U_{1-x}Am_xO_{2\pm\delta}$ sample evolutions.

*3.1.2. $U_{0.925}Am_{0.075}O_{2\pm\delta}$ and $U_{0.85}Am_{0.15}O_{2\pm\delta}$.* For the whole period of study, the diffractograms of the first two samples, $U_{0.925}Am_{0.075}O_{2\pm\delta}$ and $U_{0.85}Am_{0.15}O_{2\pm\delta}$, invariably indicate the presence of a sole fluorite phase (in addition to that of the gold reference powder). Thus, for the respective aging and accumulated doses of these samples (Table 1), $\alpha$-self-irradiation does not modify the crystalline symmetry, confirming previous observations on similar compositions[23,24] or on $AmO_{2-\delta}$,[20,37−39] and more generally the high resistance of the fluorite structure against self-irradiation.[28,40,41]

Figure 1 presents the (420) reflection of $U_{0.925}Am_{0.075}O_{2\pm\delta}$ solid solution. The evolution of this diffraction line is typical of

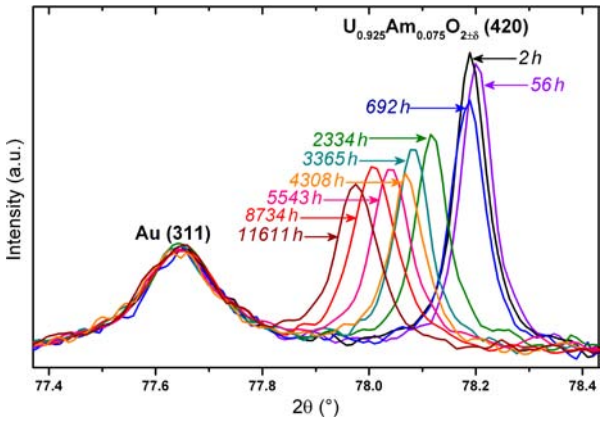


**Figure 1.** Evolution of $U_{0.925}Am_{0.075}O_{2\pm\delta}$ XRD patterns through the representative (420) diffraction peak. Similar behavior was also noted for $U_{0.85}Am_{0.15}O_{2\pm\delta}$. Normalization of diffraction line relative intensities and positions is performed using gold as a reference, as also presented herein ((311) Au peak). Background and K$\alpha_2$ Cu contributions were subtracted.

what was observed for the other diffraction lines and is also fairly representative of the evolutions of the $U_{0.85}Am_{0.15}O_{2\pm\delta}$ sample diffraction lines. The observations detailed hereafter for $U_{0.925}Am_{0.075}O_{2\pm\delta}$ are thus valid for $U_{0.85}Am_{0.15}O_{2\pm\delta}$ as well.

Since that in a large majority of cases the self-irradiation initially causes lattice swelling,[28,37,41−44] a progressive shift of the diffraction lines to lower angles is expected. A progressive shift toward higher angles is however noted during the first days (Figure 1). As further presented in section 3.3, a minimum value of unit cell parameter is obtained after around 50−100 h, whatever the sample (including those with $x \geq 0.3$), hence whatever the cumulated dose, thus suggesting that this phenomenon is not related to self-irradiation. From 50 to 100 h, this phenomenon is weakened and counterbalanced by the cell swelling due to self-irradiation. This results in the progressive shift of the diffraction lines in Figure 1, in compliance with what was initially expected. The most presumable cause of the initial cell contraction is sample oxidation in air. The initial thermal treatment, performed under a reducing $Ar/H_2(4\%)$ atmosphere, partially reduces the compounds: The oxygen content is diminished, and at least a part of the $U^{+V}$ is reduced to $U^{+IV}$.[10] After opening the furnace (thus after the return of the samples to an air atmosphere), a progressive oxidation of the samples occurs, without any changes in long-range symmetry. Since the oxidation of $MO_2$ fluorite oxides is known to lead to lattice contraction,[45] the observed initial contraction can thus be explained by the slow oxidation of the samples under air after the reducing thermal treatment.

In Figure 1, a steady decline of the diffraction peak relative intensities of $U_{0.925}Am_{0.075}O_{2\pm\delta}$ is also observed up to about 4000 h ($1.2 \times 10^{17}$ $\alpha$-decays·g$^{-1}$), after which the intensities seem to have stabilized. Beyond 4308 h, the diffraction line relative intensities are nearly half that of the first recording (2 h). For $U_{0.85}Am_{0.15}O_{2\pm\delta}$, this decrease is similar, though slower, as the peaks lost half of their relative height after the maximum recorded time of 7364 h ($4.4 \times 10^{17}$ $\alpha$-decays·g$^{-1}$). For the $U_{0.85}Am_{0.15}O_{2\pm\delta}$ sample, stabilization of diffraction line intensities was not yet reached. These relative intensity reductions are not, in both cases, accompanied by any clear peak broadening, as the full widths at half-maximum (fwhm) remain fairly stable over all experiments.

In summary, the fluorite structure remains stable for these two $U_{1-x}Am_xO_{2\pm\delta}$ samples in spite of $\alpha$ self-irradiation with cumulated doses of ~$4 \times 10^{17}$ $\alpha$·g$^{-1}$ (i.e., ~0.1 dpa). A decrease in XRD line relative intensities is, however, clear and presumably related to a partial amorphization, maybe through the formation of defect clusters.[28] As this decrease of XRD line relative intensities stop over ~4000 h for $U_{0.925}Am_{0.075}O_{2\pm\delta}$, it could further indicate that the defects associated to this progressive partial amorphization could also be self-healed, leading over a few months to an equilibrium between healing and amorphization rates, thus to the stabilization in diffractograms of the line relative intensities. In other terms, higher cumulated doses may presumably never lead to a complete amorphization of the samples, confirming the stability over time under ambient storage conditions of the fluorite $U_{0.925}Am_{0.075}O_{2\pm\delta}$ and $U_{0.85}Am_{0.15}O_{2\pm\delta}$ solid solutions.

*3.1.3. $U_{0.6}Am_{0.4}O_{2\pm\delta}$ and $U_{0.5}Am_{0.5}O_{2\pm\delta}$.* For the $U_{0.6}Am_{0.4}O_{2\pm\delta}$ and $U_{0.5}Am_{0.5}O_{2\pm\delta}$ samples, very similar evolutions were observed. The evolution of the $U_{0.6}Am_{0.4}O_{2\pm\delta}$ (220) reflection, characteristic of all other diffraction lines of both samples, is reported in Figure 2. It is first evidenced that samples are both initially composed of more than two fluorite phases. As the line positions of these phases are very close to one another, their number and characteristics could not be refined. However, this suggests that all these phases correspond to $U_{0.6}Am_{0.4}O_{2\pm\delta}$ (or $U_{0.5}Am_{0.5}O_{2\pm\delta}$) solid solutions, with close yet different $\delta$ values. During about the 100 first hours for $U_{0.6}Am_{0.4}O_{2\pm\delta}$ (15−20 h for $U_{0.5}Am_{0.5}O_{2\pm\delta}$), the relative intensities of the diffraction lines of the "low-angle" phase(s) decrease in favor of those of the "high-angle" phase(s),

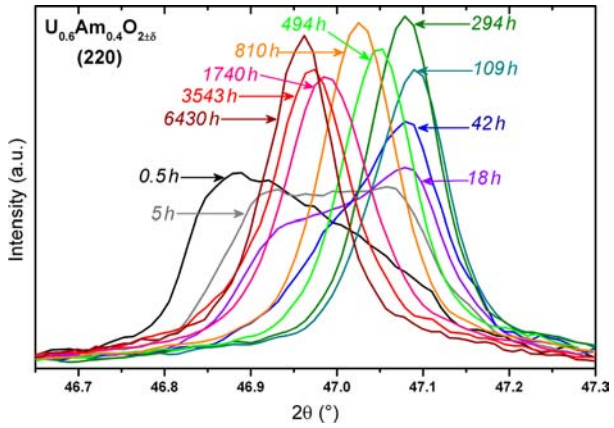


**Figure 2.** Evolution of $U_{0.6}Am_{0.4}O_{2\pm\delta}$ XRD patterns through the representative (220) diffraction line. Similar behavior was also noted for $U_{0.5}Am_{0.5}O_{2\pm\delta}$. Background and $K\alpha_2$ Cu contributions were subtracted.

which can be attributed to a global oxidation of the two samples. This eventually leads to the merging of these phases into a sole oxidized phase, thus to the restoration of a monophasic $U_{0.6}Am_{0.4}O_{2\pm\delta}$ (or $U_{0.5}Am_{0.5}O_{2\pm\delta}$) solid solution. As for the samples with lower Am content, this initial behavior is related to the atmosphere transition from that set in the furnace ($Ar/H_2(4\%)$) to that of the glove boxes (air). The most likely explanation of the observed phase evolution is the following: when the furnace is opened at the end of the heat treatment, due to the change in atmosphere, the $U_{0.6}Am_{0.4}O_{2\pm\delta}$ (or $U_{0.5}Am_{0.5}O_{2\pm\delta}$) sample is progressively oxidized. On the contrary to what was observed for the samples with $x \leq 0.15$, this oxidation brings about not only a lattice contraction, but also the formation of intermediate $U_{0.6}Am_{0.4}O_{2\pm\delta}$ (or $U_{0.5}Am_{0.5}O_{2\pm\delta}$) solid solutions with different $\delta$ values. Due to the time required for sample preparation (~0.5 h), the oxidation process is presumably already well-advanced. As a consequence, the 0.5 h diffractogram cannot be considered as representative of the $U_{0.6}Am_{0.4}O_{2\pm\delta}$ (or $U_{0.5}Am_{0.5}O_{2\pm\delta}$) sample state under $Ar/H_2(4\%)$ at room temperature, on which no information is available. Following that, the two samples might even be monophasic before the furnace opening.

While the "low-angle" phases have completely disappeared after about 100 h for $U_{0.6}Am_{0.4}O_{2\pm\delta}$ (about 15 h for $U_{0.5}Am_{0.5}O_{2\pm\delta}$), the relative intensities of the diffraction peaks corresponding to the oxidized phase continue to increase until about 300 h. In the meantime, the peak fwhm slightly decreases. This crystallinity improvement is presumably related to the progressive elimination of some (or even all) of the crystalline defects accumulated during the sample oxidation and phase transition.

After 300 h, the diffraction peak heights are maximal and, unlike those of $U_{0.925}Am_{0.075}O_{2\pm\delta}$ and $U_{0.85}Am_{0.15}O_{2\pm\delta}$ compounds, do not quantifiably diminish for longer experimental times (Figure 2). Once the oxidation process is completed, no pronounced broadening of the peaks was observed, as would also be evidenced through the Williamson–Hall peak profile analysis presented in section 3.2.

As a summary, it was found for the $U_{0.6}Am_{0.4}O_{2\pm\delta}$ and $U_{0.5}Am_{0.5}O_{2\pm\delta}$ samples that both appear stable as a fluorite solid solution under air, though the atmosphere change from $Ar/H_2(4\%)$ to air induces an oxidation and the formation of intermediate phases with a "gradient" of O/M ratios before eventually reaching a stable (or metastable) state. This peculiar oxidation behavior could be related to the existence of a miscibility gap in the U–Am–O ternary system, similar to that existing for the U–Pu–O system.[46] Another possibility is that the oxidation kinetics in these samples are different from one grain to another and/or from one crystallographic face to another. This hypothesis is, however, less probable, as similar behaviors would have been expected for the samples with lower Am contents.

On the basis of the results currently available on these compounds, a clear understanding of this oxidation behavior cannot be proposed. Dedicated studies have however been initiated notably through high temperature XRD experiments on $U_{0.5}Am_{0.5}O_{2\pm\delta}$ to try shedding light on that peculiar oxidation behavior.

*3.1.4. $U_{0.7}Am_{0.3}O_{2\pm\delta}$.* As previously stated, the $U_{0.7}Am_{0.3}O_{2\pm\delta}$ sample presents an intermediate evolution compared to the four other samples, as depicted through the evolution of the representative (200) reflection in Figure 3. From the first

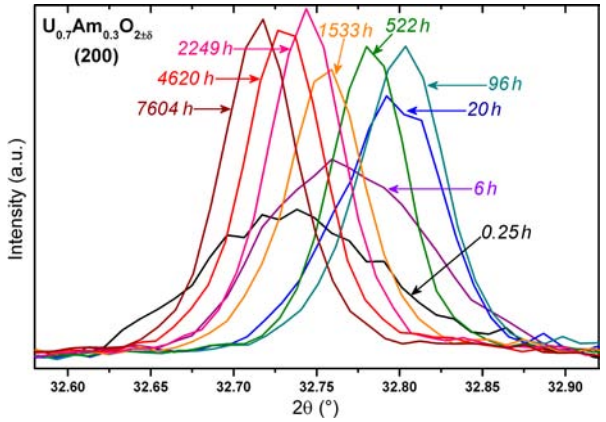


**Figure 3.** Evolution of $U_{0.7}Am_{0.3}O_{2\pm\delta}$ XRD patterns through the representative (200) diffraction line. Background and $K\alpha_2$ Cu contributions were subtracted.

recorded diffractogram, broad diffraction peaks are observed. As the diffraction peaks are roughly symmetric, this may indicate an initially reduced crystallinity of the samples, but with respect to the high temperature of heat treatment and the behavior of the compounds of similar compositions, the peak broadening is more likely attributed to the presence of several phases of $U_{0.7}Am_{0.3}O_{2\pm\delta}$ with different (but close) $\delta$ values. Between 0.5 and around 100 h, the relative heights of the diffraction lines increase while the peaks' fwhms progressively diminish. In the meantime, the diffraction lines are shifted to higher angles. These observations are more likely due to the oxidation of the different suspected fluorite phases leading eventually to the formation of a sole $U_{0.7}Am_{0.3}O_{2\pm\delta}$ fluorite phase.

Over 100 h, the $U_{0.7}Am_{0.3}O_{2\pm\delta}$ sample behaves like $U_{0.6}Am_{0.4}O_{2\pm\delta}$ and $U_{0.5}Am_{0.5}O_{2\pm\delta}$ (i.e., no trends of peak relative intensity diminution are observed) though self-irradiation provokes a lattice swelling, which is expressed in Figure 3 by the progressive shifting to low angles of the peak positions.

As a summary, for $U_{0.7}Am_{0.3}O_{2\pm\delta}$, $U_{0.6}Am_{0.4}O_{2\pm\delta}$ and $U_{0.5}Am_{0.5}O_{2\pm\delta}$ samples, once the oxidation process is completed, no modifications of the diffraction line relative intensities and shapes are noted, which leads to conclude that the crystallinity of these samples is not quantitatively affected


dx.doi.org/10.1021/ic402124s | Inorg. Chem. 2013, 52, 14196–14204

by $\alpha$ self-irradiation even for cumulated doses over $10^{18}$ $\alpha \cdot g^{-1}$ (0.2−0.3 dpa).

**3.2. Crystallite Size and Microstrain Evolutions.** It is widely reported for various compounds that both crystallite size $L$ and microstrains $<\varepsilon>$ can evolve under particle[47−51] or $\gamma$-ray[52,53] irradiation. However, we found no reports of $L$ and $<\varepsilon>$ monitoring neither for an experiment concerning $\alpha$ self-irradiation nor for one concerning an actinide oxide. This approach thus appears new for such an experimental system.

*3.2.1. Crystallite Size.* For all samples and analyzed diffractograms, Williamson−Hall plots exhibit a linear evolution of $\beta\cos\theta$ as a function of $\sin\theta$, thus indicating the isotropic shapes of crystallites, as demonstrated in the representative example in Figure 4.

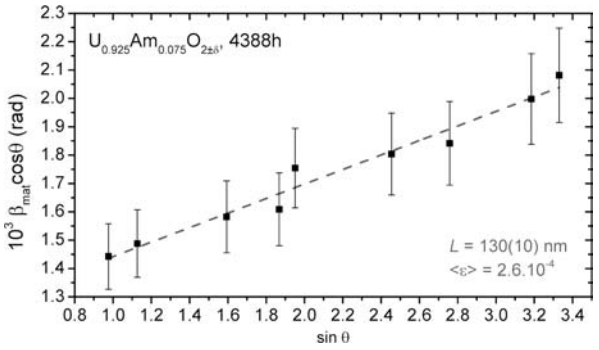


**Figure 4.** Example of application of Williamson−Hall plot for the determination of microstrain $<\varepsilon>$ and the crystallite size $L$, obtained, respectively, from the slope and the intercept of the linear fit (section 2.2.2.2).

For the compounds with $x \geq 0.15$, the determined crystallite sizes are ranging between 150 and 400 nm. For crystallite size over 150 nm, the finite size contribution to XRD peak broadening is, however, hardly detectable with the device used. Determined $L$ values are thus very imprecise. Despite this uncertainty, the crystallite size remains above 150 nm, which excludes the occurrence of a massive crystallite splitting due to $\alpha$ self-irradiation for these samples and the considered cumulated doses. This is also corroborated by the evolution of $L$ for the $U_{0.925}Am_{0.075}O_{2\pm\delta}$ sample, as $L$ has remained fairly stable ($110 \leq L \leq 140$ nm) over the duration of the experiment (1 year, cumulated dose of $3.5 \times 10^{17}$ $\alpha \cdot g^{-1}$). In summary, within the detection limit of our XRD device, a quantifiable impact of the $\alpha$ self-irradiation on the crystallite sizes of the $U_{1-x}Am_xO_{2\pm\delta}$ samples for the considered dose rates and cumulated doses was not evidenced.

*3.2.2. Microstrain.* The evolutions of microstrain for the five samples are gathered in Figure 5 as a function of the cumulated dose. For $U_{0.6}Am_{0.4}O_{2\pm\delta}$ and $U_{0.5}Am_{0.5}O_{2\pm\delta}$, the initial values of $<\varepsilon>$ could not be determined, as these samples are initially biphasic. In the meantime, for the $U_{0.925}Am_{0.075}O_{2\pm\delta}$, $U_{0.85}Am_{0.15}O_{2\pm\delta}$, and $U_{0.7}Am_{0.3}O_{2\pm\delta}$ samples, notable evolutions of $<\varepsilon>$ are observed for the first 100 h. These initial evolutions are certainly a consequence of the oxidation process, as the latter occurred during the same time lapse.

After the end of the oxidation process, the determined $<\varepsilon>$ values of each sample with $x \geq 0.15$ are found to be stabilized at average values, gathered in Table 2. These average values increase with $x$. Following this trend, $U_{0.925}Am_{0.075}O_{2\pm\delta}$ microstrain values are the lowest of the five samples, but steadily increase from $1 \times 10^{-4}$ to $3 \times 10^{-4}$ between 300 and

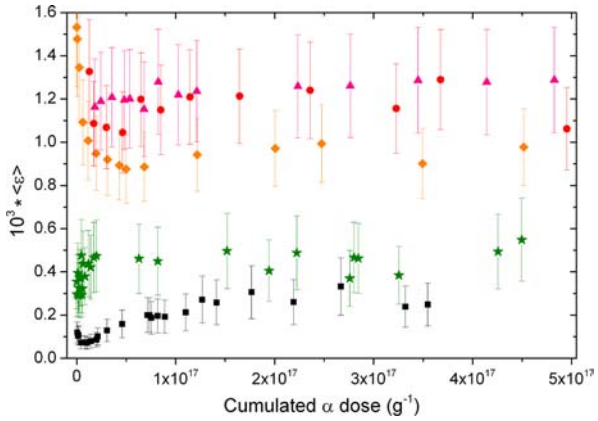


**Figure 5.** Evolution of the microstrain $<\varepsilon>$ as a function of the cumulated $\alpha$ dose for (■) $U_{0.925}Am_{0.075}O_{2\pm\delta}$, (green ★) $U_{0.85}Am_{0.15}O_{2\pm\delta}$, (orange ◆) $U_{0.7}Am_{0.3}O_{2\pm\delta}$, (red ●) $U_{0.6}Am_{0.4}O_{2\pm\delta}$, and (magneta ▲) $U_{0.5}Am_{0.5}O_{2\pm\delta}$.

**Table 2. Microstrain $<\varepsilon>$ and Crystallite size $L$ Obtained Using Williamson−Hall Plots**

| sample | considered time lapse | $10^3<\varepsilon>$ | $L$ (nm) |
|---|---|---|---|
| $U_{0.925}Am_{0.075}O_{2\pm\delta}$ | 300 to 4000 h | $0.06 + 10^{-3}t^a$ | 125(20) |
| | $t$ > 4000h | 0.3(1) | |
| $U_{0.85}Am_{0.15}O_{2\pm\delta}$ | $t$ > 300h | 0.45(10) | >150 |
| $U_{0.7}Am_{0.3}O_{2\pm\delta}$ | $t$ > 300h | 0.9(2) | >150 |
| $U_{0.6}Am_{0.4}O_{2\pm\delta}$ | $t$ > 300h | 1.1(2) | >150 |
| $U_{0.5}Am_{0.5}O_{2\pm\delta}$ | $t$ > 300h | 1.2(2) | >150 |

[a]Time $t$ expressed in days.

~4000 h (~$1.2 \times 10^{17}$ $\alpha \cdot g^{-1}$), that is, up to the moment when the diffraction line relative intensities of $U_{0.925}Am_{0.075}O_{2\pm\delta}$ stop decreasing (section 3.1.2). Over ~4000h, $<\varepsilon>$ of $U_{0.925}Am_{0.075}O_{2\pm\delta}$ stabilizes to around $3 \times 10^{-4}$.

On one hand, the increase of $<\varepsilon>$ with the americium content could be compared to the evolution of the Debye−Waller factor, which was recently determined by Prieur et al. from XAS experiments for $U_{1-x}Am_xO_{2\pm\delta}$ solid solutions ($x$ = 0.1, 0.15, and 0.2, all three compositions fabricated with the same protocol).[10] This factor, like $<\varepsilon>$, is an indicator of structural disorder, and is also found to increase with Am content. As stated by Prieur et al.,[10] the increase of $<\varepsilon>$ with $x$ is first related to the peculiar charge distribution of the $U_{1-x}Am_xO_{2\pm\delta}$ oxides (americium being exclusively present at the trivalent state, while uranium has a mixed +IV/+V valence[10−14,24]). Since the $U^{+V}$ molar fraction tends to increase with $x$, the effects of the presence of the smaller $U^{+V}$ cation on the local variation of interatomic distances consequently increase with $x$.

Another presumable contribution to the $<\varepsilon>$ increase as a function of $x$ is related to the presence of impurities. Indeed, the $AmO_{2-\delta}$ powder used for sample synthesis initially contains several impurities.[6,26] Even if the high-temperature heat treatments bring about volatilization of some of these impurities,[6] others, and notably neptunium and the lanthanide elements,[54] presumably remain in the $U_{1-x}Am_xO_{2\pm\delta}$ final oxide.[55−60] As a consequence, the presence of these impurities in substitution for Am and U (or O) or even on interstitial sites could provoke local modifications of interatomic distances and thus an increase of $<\varepsilon>$ proportional to $x$.


dx.doi.org/10.1021/ic402124s | Inorg. Chem. 2013, 52, 14196−14204

On the other hand, the difference in behavior between the samples with $x \geq 0.15$ and that with $x = 0.075$ is presumably related to the very low[47−53] initial microstrain values of the latter sample, which indicates a highly ordered structure. As a consequence, $U_{0.925}Am_{0.075}O_{2\pm\delta}$ should be more sensitive to a second-order effect, as $\alpha$ self-irradiation seems to provoke.

In summary, for the considered cumulated doses and dose rates, $^{241}$Am $\alpha$ self-irradiation does not lead to significant modifications in the sintered $U_{1-x}Am_xO_{2\pm\delta}$ sample microstrain, which instead depends on Am content.

**3.3. Unit Cell Parameter/Cell Volume Evolutions.** The relative evolutions of the unit cell parameters ($\Delta a/a_0$) and of the corresponding cell volume ($\Delta V/V_0 \approx 3\Delta a/a_0$) are plotted as a function of time in Figure 6a and as a function of the cumulated $\alpha$ dose in Figure 6b.

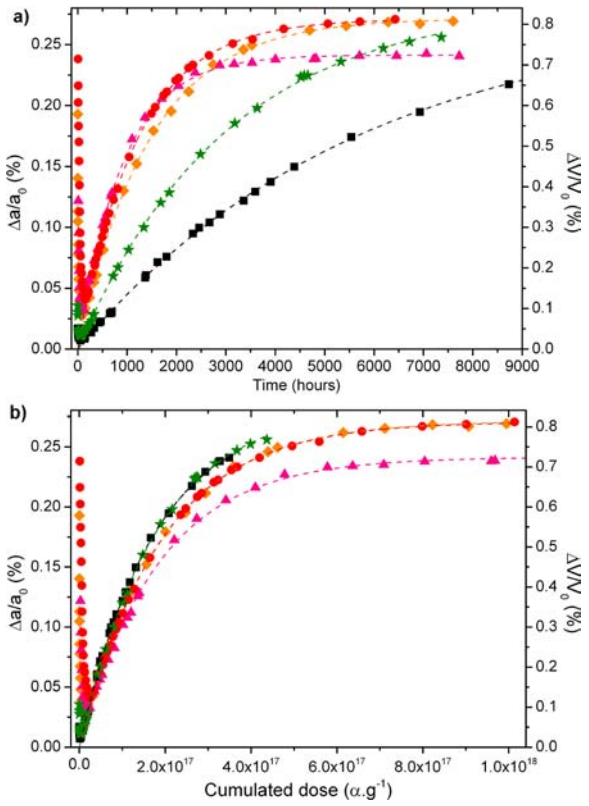


**Figure 6.** Relative evolution of unit cell parameter (or cell volume) as a function of time (a) and of the cumulated $\alpha$ dose (b) of (■) $U_{0.925}Am_{0.075}O_{2\pm\delta}$, (green ★) $U_{0.85}Am_{0.15}O_{2\pm\delta}$, (orange ◆) $U_{0.7}Am_{0.3}O_{2\pm\delta}$, (red ●) $U_{0.6}Am_{0.4}O_{2\pm\delta}$, and (magenta ▲) $U_{0.5}Am_{0.5}O_{2\pm\delta}$.

The considered $a_0$ (and $V_0$) values are calculated by regression from the $\Delta a/a_0$ evolution over ∼200 h (i.e., when sample oxidation is complete). The $a_0$ values, gathered in Table 3, thus correspond to values that would have been initially obtained if the oxidation process under air had instantaneously occurred after the furnace opening. Likewise, $a_0$ values correspond to the sample cell parameters free of any self-irradiation effects.

In Figure 6, an initial contraction of the unit cell of all samples is observed. This corresponds to the oxidation process, as oxidation of $AmO_{2-\delta}$, $UO_{2+\delta}$, or more generally of fluorite $M_{1-x}M'_xO_{2\pm\delta}$ compounds leads to a decrease of cell volume.[37,45,46,60,61] The volume contraction is maximal between 50 and 100 h and does not depend on $x$, which suggests that the oxidation kinetics are not driven by the americium content. Conversely, the amplitude of the contraction is found to increase with $x$: About 0.01% for $U_{0.925}Am_{0.075}O_{2\pm\delta}$, 0.025% for $U_{0.85}Am_{0.15}O_{2\pm\delta}$, and 0.17% for $U_{0.7}Am_{0.3}O_{2\pm\delta}$. For $U_{0.6}Am_{0.4}O_{2\pm\delta}$ and $U_{0.5}Am_{0.5}O_{2\pm\delta}$, the first hours unit cell parameters of the phase stable under air were less precisely determined because the presence of the secondary phases disturbs the refinement (though the latter are taken into account), but it was evidenced for these two compositions that the initial unit cell parameter contraction is similar or even superior to that of $U_{0.7}Am_{0.3}O_{2\pm\delta}$. As a summary, the gain of oxygen ($\Delta\delta$) during the oxidation process of the $U_{1-x}Am_xO_{2\pm\delta}$ compounds increases with Am content. This is presumably due to the fact that the higher the Am content, the more oxidation of $U^{+IV}$ to $U^{+V}$ when the sample enters in contact with air, and correspondingly the higher the $\Delta\delta$ value. It would have been quite interesting for comparison to also measure this gain by TGA (thermogravimetric analysis), but no such device integrated in a glovebox was available.

When the oxidation process is ended (over ∼200 h), the unit cell parameters of each sample increase under the sole effect of self-irradiation according to the following equation:

$$a = a_0 + K(1 - e^{-K't}) \quad (2)$$

where $K$ and $K'$ are constants. As a function of $\Delta a/a_0$, it gives:

$$\Delta a/a_0 = A(1 - e^{-B_t}) \quad (3)$$

or if the $^{241}$Am $\alpha$ cumulated dose is selected as the time scale

$$\Delta a/a_0 = A(1 - e^{-B'\alpha}) \quad (4)$$

with $A$ corresponding to the maximal expansion of the unit cell parameter, $B$ and $B'$ are constants directly related to the unit cell swelling kinetics (respectively expressed in $h^{-1}$ and g), $t$ is the time (expressed in hours), and $\alpha$ is the cumulated dose.

**Table 3. Results of Experimental Data Refinements According to Eqs 3 and 4 and Comparison to Published Results on $AmO_{2-\delta}$**

| sample [and reference] | $a_0$ (Å) | $A$ (%) | $10^4$ $B$ ($h^{-1}$) | $10^{19}$ $B'$ (g) |
|---|---|---|---|---|
| $U_{0.925}Am_{0.075}O_{2\pm\delta}$ | 5.4660(5) | 0.278(5) | 1.8 | 10.2 |
| $U_{0.85}Am_{0.15}O_{2\pm\delta}$ | 5.4609(5) | 0.284(5) | 3.3 | 9.7 |
| $U_{0.7}Am_{0.3}O_{2\pm\delta}$ | 5.4530(5) | 0.272(5) | 6.9 | 9.2 |
| $U_{0.6}Am_{0.4}O_{2\pm\delta}$ | 5.4514(5) | 0.271(5) | 8.4 | 9.2 |
| $U_{0.5}Am_{0.5}O_{2\pm\delta}$ | 5.4538(5) | 0.242(5) | 11.0 | 9.5 |
| $AmO_{2-\delta}$ [20] | 5.375(1) | 0.325 | 27.4 | 12.3 |
| $AmO_{2-\delta}$ [37] | 5.376(1) | 0.224(7) | 25.7 | 11.6 |
| $AmO_{2-\delta}$ [38] | 5.3772(4) | 0.282 | 22.3 | 10.1 |
| $AmO_{2-\delta}$ ($O_2$) [39] | 5.3774(4) | 0.239(3) | 32.2 | 14.5 |
| $AmO_{2-\delta}$ (vacuum) [39] | 5.3725(4) | 0.281(4) | 25.9 | 11.7 |


dx.doi.org/10.1021/ic402124s | Inorg. Chem. 2013, 52, 14196−14204

Such functions are commonly reported to describe the swelling under self-irradiation of unit cell dimensions of several materials,[41,44,62] including $AmO_{2-\delta}$,[20,37−39] and more generally actinide dioxides.[28,29,63,64] These functions were also recently employed to fit the increase of sintered $U_{0.85}Am_{0.15}O_{2\pm\delta}$ pellet dimensions.[24] For each sample, the fit of experimental data according to eq 3 first allowed $a_0$ values determination, which are listed in Table 3 and plotted against $x$ in Figure 7.

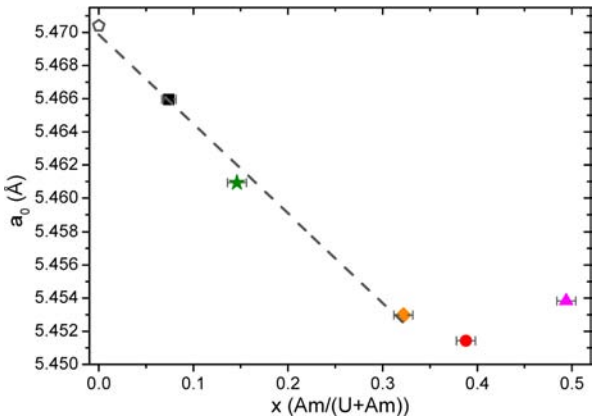


**Figure 7.** Plot as a function of Am content of the $a_0$ unit cell parameters which were obtained by regression of the experimental results of Figure 6 and using eqs 3 or 4. The unit cell parameter of $UO_2$ is taken from Lynds et al.[65]

For $0 \leq x \leq 0.3$, a linear evolution is observed. Such behavior was partly expected as previous studies on $U_{1-x}Am_xO_{2\pm\delta}$ samples prepared under similar conditions had determined an identical charge distribution within the range $0.1 \leq x \leq 0.2$:[10] Am is only present in the trivalent valence state, while U is present as a fraction $y$ of $U^{+V}$ and a fraction $1 - x - y$ of $U^{+IV}$, with $x \approx y$, leading to a $\delta$ value very close to 0, thus to an oxygen/metal (O/M) stoichiometry close to 2.0. Conversely, the obtained linear evolution of $a_0$ as a function of $x$ up to 0.3 may indicate similar or even identical oxygen stoichiometries for the $U_{0.925}Am_{0.075}O_{2\pm\delta}$, the $U_{0.85}Am_{0.15}O_{2\pm\delta}$, and the $U_{0.7}Am_{0.3}O_{2\pm\delta}$ samples. Moreover, as the obtained $a_0$ values for $U_{0.6}Am_{0.4}O_{2\pm\delta}$ and $U_{0.5}Am_{0.5}O_{2\pm\delta}$ are higher than those expected from the linear evolution in the $(0 \leq x \leq 0.3)$ range, a different cationic charge distribution and an O/M stoichiometry strictly lower than 2.0 are expected for these two samples.

The $A$, $B$, and $B'$ terms were also determined by experimental data refinement according to eqs 3 and 4 and compared to the values reported for $AmO_{2-\delta}$[20,37−39] in Table 3. For the samples with $x \leq 0.4$, very close values of $A$ around 0.28% are determined (thus corresponding to a volume increase of ∼0.8%), while a slightly lower value is calculated for $U_{0.5}Am_{0.5}O_{2\pm\delta}$ (0.242(5)%). The maximal swelling of the $U_{1-x}Am_xO_{2\pm\delta}$ compounds thus appears to be independent of or at least only slightly dependent on the Am content for the composition range studied. For $AmO_{2-\delta}$, values ranging between 0.224 and 0.325 were reported,[20,37−39] with no clear trend. This dispersion might be partially due to the lower precision of apparatus and refinement methods of the early results of refs 38 and 39 (respectively, 1968 and 1977), but it is mainly caused by the difference between impurity nature and levels, or even crystallinity and $\delta$ values. For instance, Hurtgen and Fuger[39] have already pointed out the influence of the storage atmosphere, thus of the $\delta$ value (Table 3).

Considering similar systems, $A$ values determined in this study are of the same magnitude as those published for $\alpha$ self-irradiation of $PuO_2$ (0.3%)[63] or $CmO_2$ (0.23%)[64] and are interestingly close to that determined by Kato et al. (0.29%)[29] for several $U_{1-x}Pu_xO_{2-\delta}$ solids with $x$ varying between 0.17 and 0.49.

As expected, $B$, which represents the kinetics of lattice swelling as a function of time, increases with $x$, and thus with sample activity. Moreover, the trend observed for the samples studied herein is also confirmed for $AmO_{2-\delta}$,[20,37−39] as the reported $B$ values are about twice that determined for $U_{0.5}Am_{0.5}O_{2\pm\delta}$.

Conversely, $B'$, the swelling kinetics constant determined as a function of cumulated dose, varies only slightly (from $9.2 \times 10^{19}$ to $10.2 \times 10^{19}$ g) among the samples, without any trend. For the considered composition range $(0.075 \leq x \leq 0.5)$, the Am content and thus the $\alpha$ dose rate do not influence the swelling kinetics. For $AmO_{2-\delta}$, the literature values range from $10.1 \times 10^{19}$ to $14.5 \times 10^{19}$ g[20,37−39] (i.e., to values noticeably higher than those obtained for $U_{1-x}Am_xO_{2\pm\delta}$ oxides). Therefore, an influence of composition on $B'$ cannot be ruled out for high Am contents.

## 4. CONCLUSION

The effects at the structural scale of $^{241}Am$ self-irradiation in five $U_{1-x}Am_xO_{2\pm\delta}$ ($x$ ranging between 0.075 and 0.5) compounds were studied by XRD. Prior to XRD monitoring under air, a heat treatment at 1373 K under an $Ar/H_2$ (4%) atmosphere was carried out to recover all previously accumulated structural defects. The main results of this study are summarized as follows: (1) The fluorite structure is maintained across all five experiments, confirming the stability of this structure when subject to $\alpha$-decay self-irradiation,[11,23,24,28,37−41] though consequent reductions of the diffraction line relative intensities of $U_{0.925}Am_{0.075}O_{2\pm\delta}$ and $U_{0.85}Am_{0.15}O_{2\pm\delta}$ have been noted. (2) At the end of the initial heat treatment, the change of atmosphere from reducing ($Ar/H_2$(4%)) to oxidizing (air) provokes a progressive oxidation of the samples, which is complete after at most 10 days. For the compounds with lower Am ratios, this oxidation occurred without any phase transitions, but for $U_{0.6}Am_{0.4}O_{2\pm\delta}$ and $U_{0.5}Am_{0.5}O_{2\pm\delta}$, this oxidation occurred through the progressive transition from a first fluorite $U_{0.6}Am_{0.4}O_{2\pm\delta}$ (or $U_{0.5}Am_{0.5}O_{2\pm\delta}$) solid solution to a second oxidized fluorite $U_{0.6}Am_{0.4}O_{2\pm\delta}$ (or $U_{0.5}Am_{0.5}O_{2\pm\delta}$) solid solution. (3) In the meantime and after the oxidation process, self-irradiation provokes a structural swelling up to around 0.8 vol %. Kinetic constants of swelling were also determined and were found, as expected, to be dependent on $x$, and thus on the dose rate. When the time scale is normalized by sample $\alpha$-activity, the obtained kinetic constants are however very close. (4) No significant evolutions of microstrain or crystallite size were noted, but it was evidenced that microstrain increases with $x$ as a consequence of impurities associated with both the Am starting material and the broader cationic charge distribution with increasing $x$.

In summary, the $U_{1-x}Am_xO_{2\pm\delta}$ compounds studied appeared similarly affected by self-irradiation. Moreover, $U_{1-x}Am_xO_{2\pm\delta}$ compounds stored under air are stable despite the $^{241}Am$ $\alpha$-activity as no substantial deteriorations of the fluorite structure were observed (neither amorphization (or very moderate), nor phase transition, nor crystallite splitting, nor microstrain increase). As a consequence, even though the lattice expansion result in a macroscopic swelling at the pellet scale, the structural

effects of self-irradiation are not likely to be detrimental for MABB design and preirradiation storage. Depending on the storage time considered between fabrication and irradiation, further studies might however be of interest to confirm the stability of these compounds for longer periods.

To try confirming and extending these investigations at the structural scale, complementary investigations by X-ray absorption spectroscopy and transmission electron microscopy are planned. Similarly, high-temperature XRD experiments are currently carried out for $U_{0.5}Am_{0.5}O_{2\pm\delta}$ to investigate the peculiar oxidation behavior here evidenced for the samples with high Am contents.

## AUTHOR INFORMATION


### Corresponding Author

*E-mail: thibaud.delahaye@cea.fr.


### Notes

The authors declare no competing financial interest.

## ACKNOWLEDGMENTS

The authors are thankful to M. Bataille and P. Coste for sample preparation and handling. Thanks also have to be addressed to N. Reilly and P. M. Martin for their advice. F.L. and D.H. acknowledge the CEA PACFA program for financial support through Ph.D. and postdoctoral fellowship funding, respectively.

## REFERENCES


(1) Warin, D. *J. Nucl. Sci. Technol.* **2007**, *44*, 410−414.
(2) Salvatores, M.; Palmiotti, G. *Prog. Part. Nucl. Phys.* **2011**, *66*, 144−166.
(3) Salvatores, M. *Nucl. Eng. Des.* **2005**, *235*, 805−816.
(4) Lebreton, F.; Prieur, D.; Jankowiak, A.; Tribet, M.; Leorier, C.; Delahaye, T.; Donnet, L.; Dehaudt, P. *J. Nucl. Mater.* **2012**, *420*, 213−217.
(5) Prieur, D.; Jankowiak, A.; Delahaye, T.; Herlet, N.; Dehaudt, P.; Blanchart, P. *J. Nucl. Mater.* **2011**, *414*, 503−507.
(6) Delahaye, T.; Lebreton, F.; Horlait, D.; Herlet, N.; Dehaudt, P. *J. Nucl. Mater.* **2013**, *432*, 305−312.
(7) Lebreton, F.; Prieur, D.; Horlait, D.; Delahaye, T.; Jankowiak, A.; Léorier, C.; Jorion, F.; Gavilan, E.; Desmoulière, F. *J. Nucl. Mater.* **2013**, *438*, 99−107.
(8) Prieur, D.; Lebreton, F.; Martin, P. M.; Jankowiak, A.; Delahaye, T.; Dehaudt, P.; Blanchart, P. *J. Eur. Ceram. Soc.* **2012**, *32*, 1585−1591.
(9) Lebreton, F.; Belin, R. C.; Prieur, D.; Delahaye, T.; Blanchart, P. *Inorg. Chem.* **2012**, *51*, 9369−9375.
(10) Prieur, D.; Martin, P. M.; Jankowiak, A.; Gavilan, E.; Scheinost, A. C.; Herlet, N. *Inorg. Chem.* **2011**, *50*, 12437−12445.
(11) Mayer, K.; Kanellakopoulos, B.; Naegele, J.; Koch, L. *J. Alloys Compd.* **1994**, *213*−*214*, 456−459.
(12) Nishi, T.; Nakada, M.; Suzuki, C.; Shibata, H.; Okamoto, Y.; Akabori, M.; Hirata, M. *J. Nucl. Mater.* **2011**, *418*, 311−312.
(13) Degueldre, C.; Cozzo, C.; Martin, M.; Grolimund, D.; Mieszczynski, C. *J. Solid State Chem.* **2013**, *202*, 315−319.
(14) Vespa, M.; Rini, M.; Spino, J.; Vitova, T.; Somers, J. *J. Nucl. Mater.* **2012**, *421*, 80−88.
(15) Prieur, D.; Jankowiak, A.; Leorier, C.; Herlet, N.; Donnet, L.; Dehaudt, P.; Lechelle, J.; Laval, J.-P.; Blanchart, P. *Adv. Sci. Tech.* **2010**, *73*, 104−108.
(16) Bartscher, W.; Sari, C. *J. Nucl. Mater.* **1983**, *118*, 220−223.
(17) Horlait, D.; Lebreton, F.; Delahaye, T.; Blanchart, P. *J. Am. Ceram. Soc.* **2013**, *96*, 3410−3416.
(18) Horlait, D.; Feledziak, A.; Lebreton, F.; Clavier, N.; Prieur, D.; Dacheux, N.; Delahaye, T. *J. Nucl. Mater.* **2013**, *441*, 40−46.
(19) Grandjean, S.; Arab-Chapelet, B.; Robisson, A.; Abraham, F.; Martin, P. M.; Dancausse, J.-P.; Herlet, N.; Leorier, C. *J. Nucl. Mater.* **2009**, *385*, 204−207.
(20) Prieur, D.; Jankowiak, A.; Leorier, C.; Herlet, N.; Donnet, L.; Dehaudt, P.; Maillard, C.; Laval, J.-P.; Blanchart, P. *Powder Technol.* **2011**, *208*, 553−557.
(21) D'Agata, E.; Hania, P. R.; Bejaoui, S.; Sciolla, C.; Wyatt, T.; Hannink, M. H. C.; Herlet, N.; Jankowiak, A.; Klaassen, F. C.; Lapetite, J.-M.; Boomstra, D. A.; Phelip, M.; Delage, F. *Ann. Nucl. Energy* **2013**, *385*, 204−207.
(22) Prieur, D.; Jankowiak, A.; Roudil, D.; Dubois, S.; Leorier, C.; Herlet, N.; Dehaudt, P.; Laval, J.-P.; Blanchart, P. *J. Nucl. Mater.* **2011**, *411*, 15−19.
(23) Prieur, D.; Pagliosa, G.; Spino, J.; Caciuffo, R.; Somers, J.; Eloirdi, R. *J. Solid State Chem.* **2013**, *199*, 334−337.
(24) Prieur, D.; Martin, P. M.; Lebreton, F.; Delahaye, T.; Jankowiak, A.; Laval, J.-P.; Scheinost, A. C.; Dehaudt, P.; Blanchart, P. *J. Solid State Chem.* **2012**, *194*, 206−211.
(25) Delahaye, T.; Lebreton, F. ; Prieur, D.; Coste, P.; Bataille, M.. *Procédé de préparation d'un combustible nucléaire dense à base d'au moins un actinide mineur*, French patent no. US11-60597, 2011.
(26) Lebreton, F.; Horlait, D.; Delahaye, T.; Blanchart, P. *J. Nucl. Mater.* **2013**, *439*, 99−102.
(27) Weber, W. J. *J. Nucl. Mater.* **1983**, *114*, 213−221.
(28) Weber, W. J. *Radiat. Eff. Defects Solids* **1983**, *77*, 295−308.
(29) Kato, M.; Komeno, A.; Uno, H.; Sugata, H.; Nakae, N.; Konashi, K.; Kashimura, M. *J. Nucl. Mater.* **2009**, *393*, 134−140.
(30) Takano, M.; Akabori, M.; Arai, Y. *J. Nucl. Mater.* **2011**, *414*, 174−178.
(31) Ziegler, J. F.; Ziegler, M. D.; Biersack, J. P. *Nucl. Instrum. Methods Phys. Res., Sect. B* **2010**, *268*, 1818−1823.
(32) Roisnel, T.; Rodríguez-Carvajal, J. *Mater. Sci. Forum* **2001**, *378*−*381*, 118−123.
(33) Pourghahramani, P.; Forssberg, E. *Int. J. Miner. Process.* **2006**, *79*, 106−119.
(34) Weibel, A.; Bouchet, R.; Boulc'h, F.; Knauth, P. *Chem. Mater.* **2005**, *17*, 2378−2385.
(35) Shao, Z.; Saitzek, S.; Ferri, A.; Rguiti, M.; Dupont, L.; Roussel, P.; Desfeux, R. *J. Mater. Chem.* **2012**, *22*, 9608−9612.
(36) Williamson, G. K.; Hall, W. H. *Acta. Metall.* **1953**, *1*, 22−31.
(37) Lebreton, F.; Belin, R. C.; Delahaye, T.; Blanchart, P. *J. Solid. State Chem.* **2012**, *196*, 217−224.
(38) Chikalla, T. D.; Eyring, L. *J. Inorg. Nucl. Chem.* **1968**, *30*, 133−145.
(39) Hurtgen, C.; Fuger, J. *Inorg. Nucl. Chem. Lett.* **1977**, *13*, 179−188.
(40) Matzke, Hj.; Kinoshita, M. *J. Nucl. Mater.* **1997**, *247*, 108−115.
(41) Ewing, R. C.; Weber, W. J. *The Chemistry of the Actinide and Transactinide Elements*; Springer: New York, 2011; 3813−3887.
(42) Wiss, T. *Comprehensive Nuclear Materials*; Elsevier, Ltd.: New York, 2012; Vol. 2, 465−480.
(43) Toledano, P.; Bismayer, U. *J. Phys.: Condens. Matter* **2005**, *17*, 6627−6634.
(44) Goubard, F.; Griesmar, P.; Tabuteau, A. *J. Solid State Chem.* **2005**, *178*, 1898−1902.
(45) Teske, K.; Ullmann, H.; Rettig, D. *J. Nucl. Mater.* **1983**, *116*, 260−266.
(46) Truphemus, T.; Belin, R. C.; Richaud, J.-C.; Reynaud, M.; Martinez, M.-A.; Félines, I.; Arredondo, A.; Miard, A.; Dubois, T.; Adenot, F.; Rogez, J. *Inorg. Chem.* **2013**, *432*, 378−387.
(47) Sharma, G.; Mukherjee, P.; Chatterjee, A.; Gayathri, N.; Sarkar, A.; Chakravartty, J. K. *Acta Mater.* **2013**, *61*, 3257−66.
(48) Sarkar, A.; Mukherjee, P.; Barat, P. *J. Nucl. Mater.* **2008**, *372*, 285−292.
(49) Nappé, J. C.; Monnet, I.; Grosseau, P.; Audubert, F.; Guilhot, B.; Beauvy, M.; Benabdesselam, M.; Thomé, L. *J. Nucl. Mater.* **2011**, *409*, 53−61.
(50) Novakovic, M.; Popovic, M.; Bibic, N. *Nucl. Instrum. Methods Phys. Res., Sect. B* **2010**, *268*, 2883−2887.

(51) Voronin, V. I.; Berger, I. F.; Goshchitskii, B. N. *Phys. Met. Metallogr.* **2012**, *113*, 878−882.
(52) Ramadan, A. A.; El-Shobaky, G. A.; Dessouki, A. M. *Int. J. Radiat. Appl. Instrum. C* **1989**, *34*, 787−790.
(53) El-Shabiny, A. M.; El-Shobaky, G. A.; Dessouki, A. M.; Ramadan, A. A. *Int. J. Radiat. Appl. Instrum. C* **1989**, *33*, 19−22.
(54) Zinkevich, M. *Prog. Mater. Sci.* **2007**, *52*, 597−647.
(55) Desgranges, L.; Pontillon, Y.; Matheron, P.; Marcel, M.; Simon, P.; Guimbretière, G.; Porcher, F. *Inorg. Chem.* **2012**, *51*, 9147−9149.
(56) Keller, C.; Berndt, U.; Engerer, H.; Leitner, L. *J. Solid State Chem.* **1972**, *4*, 453−465.
(57) Sibieude, F.; Foex, M. *J. Nucl. Mater.* **1975**, *56*, 229−238.
(58) Martin, P.; Ripert, M.; Petit, T.; Reich, T.; Hennig, C.; D'Acapito, F.; Hazemann, J.-L.; Proux, O. *J. Nucl. Mater.* **2003**, *312*, 103−110.
(59) Schleifer, F.; Naoumidis, A.; Nickel, H. *J. Nucl. Mater.* **1983**, *115*, 143−158.
(60) Horlait, D.; Clavier, N.; Dacheux, N.; Cavalier, R.; Podor, R. *Mater. Res. Bull.* **2012**, *47*, 4017−4025.
(61) Horlait, D.; Claparede, L.; Clavier, N.; Szenknect, S.; Dacheux, N.; Ravaux, J.; Podor, R. *Inorg. Chem.* **2011**, *50*, 7150−7161.
(62) Strachan, D. M.; Scheele, R. D. Kazelisky, A. E.; Sell, R. L. *Effects of self-irradiation from $^{238}$Pu on candidate ceramics for plutonium immobilization*. Pacific Northwest National Laboratory Report No. PNNL-14232, 2003.
(63) Chikalla, T. D.; Turcotte, R. P. *Radiat. Eff. Defects Solids* **1973**, *19*, 93−98.
(64) Noe, M.; Fuger, J. *Inorg. Nucl. Chem. Lett.* **1971**, *7*, 421−430.
(65) Lynds, L.; Youngs, W. A.; Mohl, J. S.; Libowitz, G. G. *Adv. Chem.* **1962**, *39*, 58−65.